

RoVRM: A Robust Visual Reward Model Optimized via Auxiliary Textual Preference Data

Chenglong Wang¹, Yang Gan¹, Yifu Huo¹, Yongyu Mu¹, Murun Yang¹, Qiaozhi He¹, Tong Xiao^{1,2*}, Chunliang Zhang^{1,2}, Tongran Liu³, Quan Du², Di Yang² and Jingbo Zhu^{1,2}

¹ School of Computer Science and Engineering, Northeastern University, Shenyang, China

² NiuTrans Research, Shenyang, China

³ CAS Key Laboratory of Behavioral Science, Institute of Psychology, CAS, Beijing, China

{clwang1119, zzhu8250}@gmail.com, {xiaotong, zhujingbo}@mail.neu.edu.cn

Abstract

Large vision-language models (LVLMs) often fail to align with human preferences, leading to issues like generating misleading content without proper visual context (also known as *hallucination*). A promising solution to this problem is using human-preference alignment techniques, such as best-of- n sampling and reinforcement learning. However, these techniques face the difficulty arising from the scarcity of visual preference data, which is required to train a visual reward model (VRM). In this work, we continue the line of research. We present a **Robust Visual Reward Model** (RoVRM) which improves human-preference alignment for LVLMs. RoVRM leverages auxiliary textual preference data through a three-phase progressive training and optimal transport-based preference data selection to effectively mitigate the scarcity of visual preference data. We experiment with RoVRM on the commonly used vision-language tasks based on the LLaVA-1.5-7B and -13B models. Experimental results demonstrate that RoVRM consistently outperforms traditional VRMs. Furthermore, our three-phase progressive training and preference data selection approaches can yield consistent performance gains over ranking-based alignment techniques, such as direct preference optimization.

Introduction

Large language models (LLMs) have demonstrated remarkable capabilities across various natural language processing tasks (Stiennon et al. 2020; Ouyang et al. 2022). Recent works tend to fine-tune LLMs using specialized visual instruction tuning datasets, leading to the emergence of powerful large vision-language models (LVLMs) (Liu et al. 2024a; Lin et al. 2024; Huang et al. 2024b). Despite these advancements, current LVLMs are not well-aligned with human preferences. A glaring problem is that LVLMs sometimes generate misleading content without anchoring to the given visual context (also known as *hallucination*) (Leng et al. 2024). For instance, as illustrated in Figure 1, an LVLM incorrectly identifies a “pitaya” in an image of mangosteens due to their visual similarity.

Two predominant research approaches aim to address this problem. The first approach focuses on generating richer and higher-quality visual instruction data (Li et al. 2023b;

Liu et al. 2023, 2024d), *i.e.*, annotating rich instruction samples on images of mangosteens to enable LVLMs to identify them more accurately. In contrast, a more sophisticated approach is applying human-preference alignment techniques, including best-of- n sampling and reinforcement learning (RL), which can efficiently align models with human preferences on various tasks by optimizing against a reward model without instruction samples. However, applying these alignment techniques to LVLMs is not a low-hanging fruit. It typically faces the difficulty of training a visual reward model (VRM) due to the scarcity of high-quality visual preference data (Sun et al. 2023; Yu et al. 2024a; Zhou et al. 2024b).

This work is motivated by a simple idea: human preferences are well-captured by text and these preferences can be transferred across different modalities. In this way, we can make use of rich, high-quality textual preference data in training VRMs. Building on this idea, we present a **Robust Visual Reward Model** (RoVRM), which can improve human-preference alignment for LVLMs in two ways. For one, we propose a three-phase progressive training approach to gradually bridge the task and modality gaps between textual and visual preference data, which can take full advantage of auxiliary textual preference data to improve the robustness of RoVRM. Furthermore, considering the conflict in preferences (Coste et al. 2023; Eisenstein et al. 2023), leveraging textual preference data poses a problem: not all data is beneficial for training the RoVRM. Addressing this problem, we propose an optimal transport-based preference data selection approach. This approach can select textual preference data that better aligns with the vision-language task preferences, thereby improving the efficacy of the RoVRM training process. To the best of our knowledge, we are the first to investigate the integration of preferences from different modalities.

Through experiments on five vision-language tasks, we aim to comprehensively evaluate RoVRM using two commonly used human-preference alignment techniques: best-of- n sampling and RL. Our results demonstrate improved performance in each task when aligned with reward signals from RoVRM, as confirmed by both automatic and human evaluations. Notably, when performing best-of- n sampling on the LLaVA-1.5-7B model, RoVRM outperforms a traditional VRM by 8.4 points on the LLaVA-Bench benchmark.

*Corresponding author.

As another bonus, our three-phase progressive training and preference data selection can be seamlessly integrated with arbitrary ranking-based alignment techniques, such as direct preference optimization (DPO) (Rafailov et al. 2024), SimPO (Meng, Xia, and Chen 2024), and ORPO (Hong, Lee, and Thorne 2024). For instance, on the LLaVA-1.5-13B model, integrating with DPO results in an additional improvement of 17.82 points on the MM-Instruct benchmark compared to standard DPO.

Related Work

In recent years, LVLMs have served as the primary backbone for vision-language tasks (Achiam et al. 2023; AI 2023). Aligning LVLMs with human preferences is effective in gaining more performance (Liu et al. 2023; Wang et al. 2024c). However, in this process, they only used visual preference data and never leveraged the textual preference data that exists in abundance.

Large Vision-Language Models Inspired by the success of LLMs such as GPTs (Brown et al. 2020; Ouyang et al. 2022) and LLaMA (Touvron et al. 2023), researchers have been aiming to develop LVLMs. The basic idea is to augment LLMs with visual inputs (e.g., images) to provide an interface for vision-language tasks (Alayrac et al. 2022; Awadalla et al. 2023; Aiello et al. 2023). Recent works on LVLMs could be classified into two groups. The first group focused on integrating visual information into LLMs (Chen et al. 2023; Liu et al. 2024a; Wang et al. 2024d). For example, Liu et al. (2024c) constructed a large amount of visual instruction data to pre-train the visual projection layer. Lin et al. (2024) further investigated the effective pre-training design options to augment LVLMs. The second group that has attracted attention commonly aimed to improve the consistency of output text and visual content, particularly addressing the problem of hallucination (Zhou et al. 2023; Leng et al. 2024; Gunjal, Yin, and Bas 2024; Huang et al. 2024a; Favero et al. 2024). This work belongs to the latter, where our RoVRM can improve the consistency of output text and visual content.

Human-Preference Alignment for LVLMs Reinforcement learning with human feedback (RLHF) has been shown to effectively align LLM behaviors with human preferences (Stiennon et al. 2020; Ouyang et al. 2022). Several works have improved RLHF by using fine-grained reward models (Wu et al. 2024), reward model ensembles (Coste et al. 2023), and direct preference optimization objectives (Rafailov et al. 2024). Additionally, some works focused on generating large, high-quality textual preference datasets to further improve RLHF in LLMs (Cui et al. 2023; Dubois et al. 2024). In the context of LVLMs, existing works mainly focused on the adaptation of the human-preference alignment techniques (Sun et al. 2023; Li et al. 2023a; Yu et al. 2024a). A significant challenge here was the scarcity of visual preference data. To address this challenge, many efforts have been made to create visual preference data, including collecting human preferences (Sun et al. 2023), and acquiring preferences from a strong LVLM (Li et al. 2023a; Yu et al. 2024b). Different from these works, we investigate

how to leverage rich, high-quality textual preference data to offset the scarcity of visual preference data.

Our Method

We first review the preliminaries of the human-preference alignment training for language models. Then, we present the three-phase progressive training for use with RoVRM. Last, we introduce the proposed preference data selection.

Preliminaries

Reinforcement Learning with Human Feedback RLHF is a key technique for aligning language models with human preferences. It typically consists of two main steps: 1) training a reward model (also known as preference model) from preference data, and 2) using an RL algorithm, such as PPO (Schulman et al. 2017), to maximize the reward. In step 1, we usually employ the Bradley-Terry model (Bradley and Terry 1952). When the preference data existed in a comparison pair, the loss function can be written as:

$$\mathcal{L}_{\text{reward}} = -\log(\sigma(r_\theta(x, y_w) - r_\theta(x, y_l))) \quad (1)$$

where σ is the Sigmoid activation function, $r(\cdot)$ is a reward model and θ is its parameters. y_w and y_l are two different responses for the human prompt x , where y_w is more preferred than y_l . When dealing with multiple responses more than two, we can induce $\mathcal{L}_{\text{reward}}$ based on the more general Plackett-Luce model (Luce 2005):

$$\mathcal{L}_{\text{reward}} = -\sum_{i=1}^k \log \frac{\exp(r_\theta(x, y_i))}{\sum_{j=i}^k \exp(r_\theta(x, y_j))} \quad (2)$$

where k denotes the number of responses. These responses are ranked by the defined preferences: $(y_1 \succ \dots \succ y_k | x)$, where y_1 is the best while y_k is the worst. In step 2, the reward signals produced by the trained reward model are instrumental in adjusting the parameters of the language models. Thus, the alignment of the language model is significantly influenced by how well the reward model is trained.

Direct Preference Optimization To bypass the complex RL procedure, Rafailov et al. (2024) proposed the direct preference optimization (DPO) which employs a reward model training objective to maximize rewards. It gives a new loss function:

$$\mathcal{L}_{\text{DPO}} = -\log \sigma[\beta \log(\frac{p_{\theta'}(y_w|x)}{p_{\theta'_{old}}(y_w|x)}) - \beta \log(\frac{p_{\theta'}(y_l|x)}{p_{\theta'_{old}}(y_l|x)})] \quad (3)$$

where θ' denotes the parameters of the language model, θ'_{old} denotes the parameters of the language model trained via supervised fine-tuning, β denotes a scaling factor, and σ denotes a Sigmoid function.

Best-of- n Sampling Best-of- n sampling (also known as re-ranking) refers to reordering or reevaluating a set of candidate responses sampled from a trained model (Lee, Auli, and Ranzato 2021; Fernandes et al. 2022). Given a set \mathcal{Y} of n candidate responses for x , we can also use the best-of- n sampling approach to maximize the reward, thereby aligning the response with human preferences. Typically, we employ

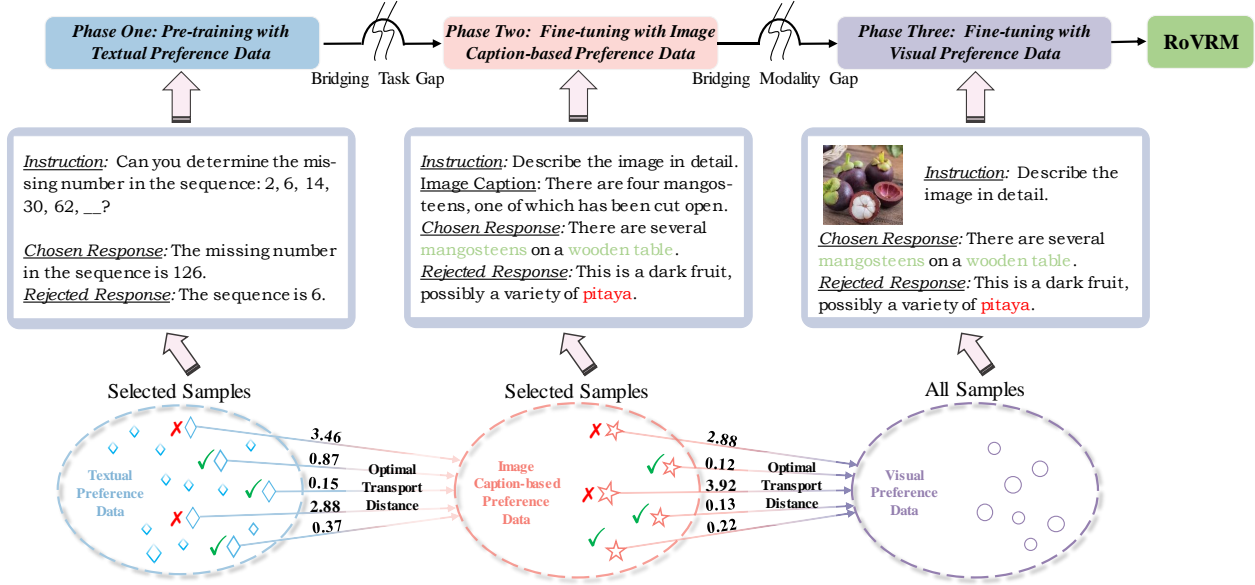


Figure 1: We propose three-phase progressive training and optimal transport-based preference data selection approaches to train RoVRM. For three-phase progressive training, we take full advantage of textual preference data to compensate for the limited availability of visual preference data. Using this preference selection, samples for phases one and two are selected based on those selected for the subsequent phase. \checkmark denotes a selected sample, while \times denotes one that is not selected.

the reward model to score the candidate responses and select a final response that has a maximum reward score.

We can notice that when applying these alignment training methods to LVLMs, sufficient visual preference data is required either to train a VRM or to perform DPO training. However, in practice, visual preference data is often insufficient and expensive to acquire.

A Robust Visual Reward Model

We aim to provide a RoVRM for human-preference alignment in LVLMs. The overview of training RoVRM is depicted in Figure 1. As shown in the figure, we present a three-phase progressive training and preference data selection to improve the robustness of RoVRM.

Three-Phase Progressive Training In response to the scarcity of visual preference data, we propose a three-phase progressive training approach that effectively solves this issue. Phase one is to conduct preference pre-training using a large amount of textual preference data. This phase can help our RoVRM to pre-learn general preferences. Ideally, the RoVRM would inherit these general preferences when processing vision-language tasks. However, this faces two serious obstacles: *task gap* and *modality gap*, which prevent these preferences from being directly applicable to vision-language tasks (see experiments in Figure 4). Here, we design phases two and three to bridge these gaps progressively. Phase two is to bridge the task gap by constructing vision-language preference data based on image captions and fine-tuning the RoVRM. Specifically, we use image captions to replace the images for visual preference data, *i.e.*, changing the human prompt $x=[\text{Instruction}; \text{Image}]$ to $x=[\text{Instruction}; \text{Image Caption}]$ in Eqs. 1 and 2. Building on phase two, phase three is to bridge the modal-

ity gap by using the visual preference data to continue fine-tuning the RoVRM with a visual projector. Compared to training a VRM directly with visual preference data, this three-phase training process incurs additional time costs due to an extra preference training session. However, it can leverage auxiliary textual preference data to improve robustness and respond to the scarcity of visual preference data. Furthermore, although pre-training followed by fine-tuning is widely used in machine learning (Devlin et al. 2019; Liu et al. 2019b; Xiao and Zhu 2023), our approach is the first to demonstrate the feasibility of optimizing a VRM through this paradigm.

Preference Data Selection Not all preference data aligns with the preferences used in subsequent phases, and conflicts may arise. Thus, during each training phase, we expect to employ samples that more closely align with the preferences contained in the data for the next phase. To achieve this, we propose an optimal transport-based preference data selection approach. We apply this approach to perform preference data selection for phases one and two, based on the preference data used in the next phase. For instance, in phase one, following Xia et al. (2024)'s work, we first extract gradient features for all samples in the textual preference dataset $\mathcal{D}_T = \{s_1^t, s_2^t, \dots, s_m^t\}$. Based on these features, we compute the distance score between each sample in \mathcal{D}_T and the image caption-based preference dataset $\mathcal{D}_C = \{s_1^c, s_2^c, \dots, s_n^c\}$ using optimal transport. The details are described as follows.

Gradient Feature. Xia et al. (2024) construct gradient features for each sample of general supervised fine-tuning data to select the data that more effectively improves the specific downstream task. Here, using these gradient features, we conduct the preference data selection. Specifically, we firstly

use LoRA (Hu et al. 2022) to efficiently perform a warmup reward model training with a small subset of preference data $\mathcal{D}_{\text{Warmup}}$, where $\mathcal{D}_{\text{Warmup}}$ is a subset extracted randomly from $\mathcal{D}_{\text{T}} \cup \mathcal{D}_{\text{C}}$. Then, we extract the gradient features for each preference sample in \mathcal{D}_{T} and \mathcal{D}_{C} through the forward and backpropagating on the warmed-up reward model:

$$g = \text{RP}(\nabla \mathcal{L}_{\text{reward}}(s; \theta_{\text{warmup}})) \quad (4)$$

where g is the gradient feature of the preference sample s and θ_{warmup} is the parameters of the warmed-up reward model. $\text{RP}(\cdot)$ is a random projection (Xie, Li, and Xue 2017) that reduces the dimensionality of gradient features.

Optimal Transport-based Distance. Unlike the Xia et al. (2024) who use the cosine similarity to compute sample distance scores, we use optimal transport (Villani et al. 2009), endowed with the capability to compute the distance transferring an arbitrary data feature to a specific data feature (Gurumoorthy, Jawanpuria, and Mishra 2021; Kang et al. 2024). Our motivation is to gather preference data for easy integration into the next training phase. To reduce computational overhead, we select a representative subset $\mathcal{D}_{\text{SubC}}$ from \mathcal{D}_{C} . This subset approximates the distance computation for the entire dataset \mathcal{D}_{C} when selecting samples from \mathcal{D}_{T} . We define the distance score of i -th sample in \mathcal{D}_{T} by:

$$c_i = \frac{1}{|\mathcal{D}_{\text{SubC}}|} \sum_{j=1}^{|\mathcal{D}_{\text{SubC}}|} \text{OT}(g_i^t, g_j^c) \quad (5)$$

where g_i^t and g_j^c denote the gradient features for the preference samples s_i^t and s_j^c , respectively. $\text{OT}(\cdot)$ denotes the function of computing the transfer distance. Given gradient features g_i^t, g_j^c over a gradient space \mathcal{Z} , the optimal transport-based transfer distance can be defined as:

$$\text{OT}(g_i^t, g_j^c) := \min_{\gamma \in \Gamma(g_i^t, g_j^c)} \int_{\mathcal{Z}^2} C(z, z') d\gamma(z, z') \quad (6)$$

where $C(\cdot)$ denotes a symmetric positive-definite cost function, and $\Gamma(g_i^t, g_j^c)$ denotes a collection of couplings between two gradients g_i^t and g_j^c . Here, we utilize L_2 -norm as the cost function and define the sum of the solved γ as the distance score. A lower distance score indicates that the textual preference sample has preferences more easily transferable to the vision-language task. Our implementation of optimal transport solvers is done using Python Optimal Transport (POT)*. While optimal transport distance has been used in data selection before (Kang et al. 2024), this is the first application to preference data selection.

To ensure that the ultimate goal of selecting preference data is to transfer preferences from textual preference data to vision-language tasks, we start by selecting image caption-based preference data for phase two. Next, we choose the textual preference data for phase one based on the preference data selected in phase two.

Experiments

We evaluated our RoVRM on the commonly used vision-language tasks based on the best-of- n sampling and rein-

forcement learning (RL). We also evaluated our approaches to direct preference optimization (DPO).

Experimental Setups

Datasets The datasets used in this work are as follows:

- *Textual Preference Dataset*: We used UltraFeedback (Cui et al. 2023), a large-scale, high-quality, and diversified preference dataset, as our textual preference dataset. It comprises 64k instructions, each with 4 responses, leading to over 340k comparison preference pairs.
- *Image Caption-based Preference Dataset*: We constructed an image caption-based preference dataset to bridge the task gap. Specifically, we employed GPT-4o-mini to generate detailed image captions that replace the visual content in our preference data. Note that when the image is present in the COCO caption dataset†, we used the human-annotated captions directly.
- *Visual Preference Dataset*: We employed the visual preference dataset from RLAIF-V (Yu et al. 2024b), which consists of about 83k comparison preference pairs. To our knowledge, it is the largest scale open source preference dataset in computer vision.
- *RL Training*: We sampled 50k instructions from LLaVA-Instruct-150K (Liu et al. 2024c) for training.

Settings For training RoVRM, we used the LLaVA-1.5-7B model to initialize the visual reward model. The learning rates for the three-phase progressive training were set to 2e-5 for phase one, and 1e-6 for phases two and three. For optimal transport-based preference data selection, we used 5k samples to warm up the VRM, consisting of 2k samples from the dataset to be selected and 3k samples from the target preference dataset. The representative subset size was set to 5k samples. For best-of- n sampling and RL training, we employed the LLaVA-1.5-7B as the initial model. In the process of best-of- n sampling, we set the sampling size to 8. We also tested other sampling sizes in Figure 5. More training settings are shown in Appendix A.

Evaluation We evaluated the RoVRM in two key aspects: trustworthiness, which denotes the level of hallucination, and helpfulness, which reflects overall interaction capability. Trustworthiness was evaluated using three benchmarks: Object HalBench (Rohrbach et al. 2018), MMHal-Bench (Sun et al. 2023), and AMBER (Wang et al. 2023). We reported the response-level (**Resp.**) and mention-level (**Ment.**) hallucination rates in the Object HalBench. GPT-4 was employed to evaluate the response-level hallucination rate (**HalRate**) and informativeness score (**Score**) on the MMHalBench. Additionally, we provided the object coverage (**Cover.**) and hallucination rate metrics for AMBER. To assess helpfulness, we used two benchmarks: MM-Instruct (Liu et al. 2024d) and LLaVA-Bench (In-the-Wild) (Liu et al. 2024c). GPT-4, following the settings in lmms-eval‡, was used to score responses in LLaVA-Bench. For MM-Instruct, responses from LLaVA-1.5-13B were used as a baseline, and

†<https://huggingface.co/datasets/lmms-lab/COCO-Caption2017>

‡<https://github.com/EvolvingLMMs-Lab/lmms-eval>

*<https://pythonot.github.io/index.html>

Method	#Param	MMHalBench		Object HalBench		AMBER		LLaVA ^W	MMIns
		Score \uparrow	HalRate \downarrow	Resp. \downarrow	Ment. \downarrow	Cover. \uparrow	HalRate \downarrow	Score \uparrow	WinRate \uparrow
GPT-4V (Achiam et al. 2023) [‡]	-	3.49	28.1	13.6	7.3	67.1	30.7	93.1	100.00
GPT-4o	-	3.58	26.0	10.7	5.2	64.0	24.9	126.4	100.00
GPT-4o-mini	-	3.02	29.2	9.1	5.4	58.4	18.5	130.9	100.00
Qwen-VL-Chat (Bai et al. 2023) [‡]	10B	2.76	38.5	40.4	20.7	53.2	31.0	71.9	73.58
OmniLMM (Hu et al. 2023) [†]	12B	3.14	36.5	12.2	6.2	-	-	72.7	-
MiniGemini (Li et al. 2024) [†]	34B	3.08	38.5	14.5	8.0	-	-	79.2	-
LLaVA-NeXT (Liu et al. 2024b) [†]	34B	3.31	34.4	12.6	6.4	63.2	43.6	77.7	93.83
LLaVA-1.5-7B (Liu et al. 2024a) ^{‡‡}	7B	2.36	51.0	53.6	25.2	51.8	34.7	65.4	-
LLaVA-1.5-13B (Liu et al. 2024a) [‡]	13B	2.42	-	46.3	22.6	-	-	72.5	-
LURE (Zhou et al. 2023) [†]	7B	1.64	60.4	27.7	17.3	-	-	36.9	-
HA-DPO (Zhao et al. 2023) [†]	7B	1.98	60.4	39.9	19.9	49.5	29.1	60.3	-
VCD (Leng et al. 2024) [†]	7B	2.12	54.2	48.8	24.3	51.5	39.0	65.8	42.56
Silkie (Li et al. 2023a) [†]	10B	3.19	32.3	27.1	13.4	56.0	28.4	73.2	63.64
LLaVA-RLHF (Sun et al. 2023) [†]	13B	2.02	62.5	38.1	18.9	52.0	39.2	61.5	74.24
RLHF-V (Yu et al. 2024a) [†]	13B	2.45	51.0	12.2	7.5	-	-	51.4	-
Best-of-n Sampling									
LLaVA-1.5-7B	7B	2.12	55.0	50.3	29.0	50.3	37.1	66.7	46.16
+VRM-Vanilla	7B	2.39	47.9	35.3	21.2	50.8	29.0	73.6	57.69
+RoVRM-Random	7B	2.52	43.8	32.7	18.9	51.7	26.9	77.2	58.49
+RoVRM	7B	2.68	40.6	30.4	16.8	53.2	23.9	82.0	61.91
LLaVA-1.5-13B	13B	2.30	53.8	49.0	25.8	50.6	37.2	75.6	50.00
+VRM-Vanilla	13B	2.41	51.0	32.7	16.7	51.4	26.6	84.0	73.08
+RoVRM-Random	13B	2.43	48.3	29.0	15.7	51.9	25.7	86.4	74.42
+RoVRM	13B	2.57	47.3	26.8	13.1	53.6	22.8	89.8	78.75
Reinforcement Learning									
LLaVA-1.5-7B	7B	2.12	55.0	50.3	29.0	50.3	37.1	66.7	46.16
+VRM-Vanilla	7B	2.17	53.2	37.7	26.0	49.1	29.1	72.8	51.11
+RoVRM-Random	7B	2.21	50.8	31.3	22.0	48.7	24.3	74.2	54.35
+RoVRM	7B	2.36	48.9	27.0	16.3	48.2	23.4	78.3	58.69
LLaVA-1.5-13B	13B	2.30	53.8	49.0	25.8	50.6	37.2	75.6	50.00
+VRM-Vanilla	13B	2.49	50.0	27.8	16.1	41.1	23.2	78.2	52.63
+RoVRM-Random	13B	2.34	47.9	31.7	15.3	48.6	21.0	79.5	60.53
+RoVRM	13B	2.57	43.8	25.0	13.2	47.7	19.5	81.7	65.79

Table 1: Experimental results on different vision-language tasks. The best results for each group are in **bold**. Results marked with \dagger for MMHalBench, Object HalBench, and LLaVA^W are from Yu et al. (2024b). Results marked with \ddagger for AMBER are from Wang et al. (2024c). Results marked with $\ddagger\ddagger$ for LLaVA^W are from Liu et al. (2024a). The other baseline results are obtained by testing this available model or using the provided API.

we computed the win rate (**WinRate**) as per Liu et al. (2024d). Additionally, a human evaluation was conducted to validate further RoVRM’s effectiveness.

Baselines Our baseline were the **LLaVA-1.5-7B** and **-13B** models without human-preference alignment. We also compared with other general LVLMs, such as **GPTs** (Achiam et al. 2023) and **Qwen-VL-Chat** (Bai et al. 2023). Furthermore, we compared RoVRM with commonly used methods to solve the hallucination, including **LURE** (Zhou et al. 2023), **HA-DPO** (Zhao et al. 2023), and others. The traditional VRM training was also our baseline, where we optimized a VRM only using our visual preference dataset (**VRM-Vanilla**). To evaluate the effectiveness of optimal transport in preference data selection, we chose **RoVRM-Random** as a baseline. In RoVRM-Random, we randomly selected samples during the preference data selection.

Experimental Results

Results of Best-of- n Sampling Table 1 summarizes the performance of our RoVRM on the best-of- n sampling. On all vision-language tasks, RoVRM consistently outperforms the VRM-Vanilla which does not use textual preference data. For instance, when using the LLaVA-1.5-7B model, RoVRM can outperform VRM-Vanilla by 8.4 points on the LLaVA-Bench. We also observe this consistent phenomenon on the LLaVA-1.5-13B model. Moreover, from the results, we find that RoVRM significantly reduces visual hallucinations, *e.g.*, lowering the hallucination rate by 13.2 points in the LLaVA-1.5-7B model. We attribute this improvement to the extensive use of textual preference data, which improves VRM’s capacity to evaluate facticity. Interestingly, we also find that RoVRM enables the LLaVA-1.5 models to outperform stronger LVLMs, with the LLaVA-1.5-7B model even surpassing the LLaVA-1.5-13B model on most of the benchmarks, such as MMHalBench and LLaVA-

Method	AMBER		LLaVA ^W	MMIns
	Cover. \uparrow	HalRate \downarrow	Score \uparrow	WinRate \uparrow
LLaVA-1.5-7B	50.3	37.1	66.7	46.16
Best-of-n Sampling				
RoVRM	53.2	23.9	82.0	61.91
w/o PDS	52.4	25.1	80.6	61.36
w/o TPT-One	51.0	26.7	71.3	59.52
w/o TPT-Two	51.8	24.9	78.0	54.76
Reinforcement Learning				
RoVRM	48.2	23.4	78.3	58.69
w/o PDS	46.2	32.2	75.2	53.70
w/o TPT-One	44.3	35.0	73.0	51.85
w/o TPT-Two	47.5	28.2	76.1	55.56

Table 2: The suffixes “-One” and “-Two” denote the removal of phases one and two, respectively, in the three-phase progressive training approach. “w/o PDS” denotes that all data is used for each training phase without employing preference data selection. **PDS**: preference data selection; **TPT**: three-phase progressive training.

Bench. This finding shows a promising direction for achieving *weak-to-strong generalization* (Burns et al. 2023).

Results of Reinforcement Learning Compared to best-of- n sampling, RL typically requires a more robust reward model: The reward model not only evaluates responses as “good” or “bad” but also provides an accuracy score margin between the responses (Zhou et al. 2024a). From the results, we find that RoVRM fulfills this requirement more effectively than VRM-Vanilla, resulting in improved RL training performance in LVLMs. For instance, in RL training on the LLaVA-1.5-7B model, RoVRM surpasses VRM-Vanilla by 7.58 points on MM-Instruct. This finding demonstrates that RoVRM is robust and can deliver high-quality reward signals across various alignment techniques. Additionally, we observe that RL training reduces hallucinations but slightly decreases the “Cover.” metric, which is consistent with the findings of Meng, Xia, and Chen (2024)’s work and DPO training in Table 3. We conjecture that preference alignment training may slightly hurt the instruction-following capability of LVLMs (Wang et al. 2024a).

Furthermore, compared to RoVRM-Random, RoVRM shows better performance across all benchmarks. This indicates that optimal transport-based preference data selection outperforms random selection. However, RoVRM-Random also significantly improves performance over VRM-Vanilla. We attribute this to the fact that RoVRM-Random also collects some textual preference data when training a VRM.

Ablation Study

We present detailed ablation studies to investigate the effects of three-phase progressive training and our preference data selection approach. The experiments are conducted on the LLaVA-1.5-7B model and the impacts of removing each approach were thoroughly examined. Furthermore, we study the impact of eliminating the distinct designs of phases one and two. The results are summarized in Table 2. Through the results, we can see that three-phase progressive training

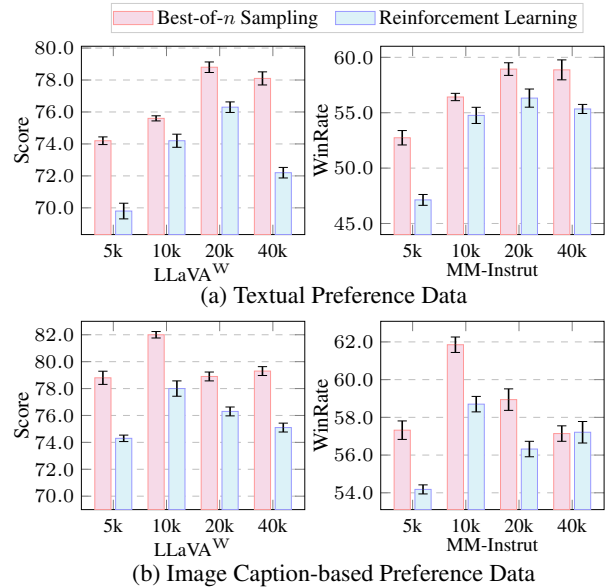


Figure 2: We train RoVRM with varying amounts of textual and image caption preference data. Experiments are conducted on the LLaVA-1.5-7B model using three different seeds, and we report the average results along with their standard deviation.

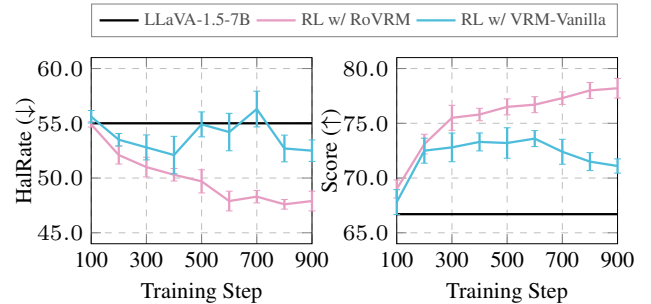


Figure 3: Performance during RL training is evaluated on the MMHalBench (left) and LLaVA-Bench (right) benchmarks using three different seeds.

significantly improves the performance of RoVRM in both best-of- n sampling and RL. Notably, removing phase one leads to a substantial performance decline (e.g., a loss of 10.7 points on the LLaVA-Bench for best-of- n sampling), highlighting the importance of textual preference data in training RoVRM. Likewise, removing image caption-based preference data also results in performance loss, indicating the need to address the task gap. Additionally, we see that using the preference data selection can train a better RoVRM. It shows the effectiveness of using optimal transport to conduct preference data selection.

Analysis

Performance on Different Numbers of Selected Preference Samples We investigate the impact of different numbers of selected preference samples using a three-phase progressive training with LLaVA-Bench and MM-Instruct. We test sample sizes of 5k, 10k, 20k, and 40k, alongside 20k

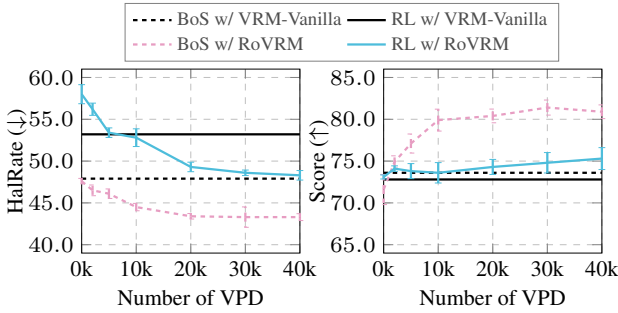


Figure 4: Performance of best-of- n sampling (BoS) and RL on MMHalBench (left) and LLaVA-Bench (right) across three different seeds. The RoVRM model is trained with varying amounts of visual preference data (VPD): 0k, 1k, 5k, 10k, 20k, 30k, and 40k.

Method	AMBER		LLaVA ^W	MMIns
	Cover. \uparrow	HalRate \downarrow	Score \uparrow	WinRate \uparrow
LLaVA-1.5-7B	50.3	37.1	66.7	46.16
+DPO	49.6	22.2	80.9	56.09
+RoDPO	50.7	17.6	83.7	73.91
LLaVA-1.5-13B	50.6	37.2	75.6	50.00
+DPO	49.2	15.7	84.2	65.63
+RoDPO	49.8	12.8	86.4	78.72

Table 3: Performance on the direct preference optimization.

image caption-based preference samples (Figure 2(a)). Our results show that using 20k textual preference samples yields strong performance, even outperforming the 40k sample scenario. Consequently, we choose 20k textual preference samples for phase one to train our RoVRM. Similarly, we evaluate sample sizes of 5k, 10k, 20k, and 40k for phase two, *i.e.*, image caption-based preference data selection (Figure 2(b)), identifying 10k as the optimal sample size.

Comparison of RL Training Process on Different VRMs Figure 3 illustrates the performance of the LLaVA-1.5-7B model comparing RL training with VRM-Vanilla and RoVRM. The results show that RL training with RoVRM improves performance more effectively than VRM-Vanilla. Additionally, we observe that RoVRM can lead to a more stable RL training process by mitigating reward over-optimization (Gao, Schulman, and Hilton 2023).

Enabling Few-Shot Learning in VRM Figure 4 shows RoVRM’s performance with different numbers of visual preference data. Note that when the visual preference dataset is small (*i.e.*, 1k, 5k, and 10k), we use the entire dataset without image caption-based preference data selection. From the results, we find that pre-training with textual preference data enables effective few-shot learning in VRM (Wang et al. 2020). Based on these textual preferences, the reward model quickly generalizes to vision-language tasks using only a few visual preference samples. Notably, using only 5k visual preference samples can achieve a performance comparable to that of VRM-Vanilla trained with 83k samples. However, while it is feasible to directly use a textual reward model (*i.e.*, using 0k visual preference data) to optimize LVLM,

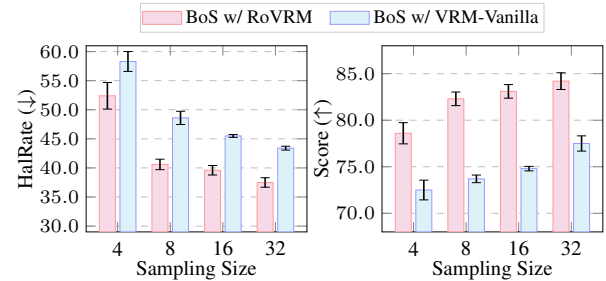


Figure 5: Performance of best-of- n sampling (BoS) with different sampling sizes: 4, 8, 16, and 32.

Evaluation Result	Best-of- n Sampling		Reinforcement Learning	
	LLaVA ^W	MMIns	LLaVA ^W	MMIns
RoVRM is better	27	33	25	44
VRM-Vanilla is better	12	23	15	23
Tie	21	43	20	32
P-value	0.0133		0.0035	

Table 4: The results of human evaluation. We report the statistical significance of the differences between the RoVRM and VRM-Vanilla models using the McNemar test.

the results are worse, particularly during RL training.

Integration with Direct Preference Optimisation Despite bypassing reward model training, direct preference optimization (DPO) still requires preference data to train the language model with a ranking-loss function. Consequently, DPO also faces the challenge of limited visual preference data in LVLMs. To address this, we propose a **Robust DPO** (namely RoDPO) by integrating our three-phase progressive training and preference data selection. Our experiments on the LLaVA-1.5-7B and -13B models show that RoDPO performs better than DPO, as summarized in Table 3.

Performance on Different Sampling Sizes We evaluate the performance of best-of- n sampling with varying sample sizes using the LLaVA-1.5-7B model. Figure 5 presents a comparison of RoVRM and VRM-Vanilla on the MMHalBench (left) and LLaVA-Bench (right) benchmarks. The experimental results indicate that RoVRM consistently enhances performance across different sampling sizes, highlighting its improved robustness.

Human Evaluation In addition to automatic evaluation, we have conducted a comparative human evaluation of RoVRM and VRM-Vanilla on the LLaVA-1.5-7B model. Two independent evaluators, who remained anonymous, assessed the responses generated by these models for the same set of image-question pairs. The results of this evaluation are presented in Table 4. These findings align with the outcomes of the automatic evaluation, demonstrating that our RoVRM consistently outperforms VRM-Vanilla. The statistically significant differences observed between the two models further underscore the distinct advantages of RoVRM.

See more analysis in **Appendix B**.

Conclusion

In this paper, we focus on improving the human-preference alignment for LVLMs. We present a **Robust Visual Reward Model** (namely RoVRM) via three-phase progressive training and preference data selection approaches. Our extensive experiments demonstrate that our RoVRM significantly outperforms the traditional visual reward model.

Acknowledgments

This work was supported in part by the National Science Foundation of China (Nos. 62276056 and U24A20334), the Natural Science Foundation of Liaoning Province of China (2022-KF-26-01), the Fundamental Research Funds for the Central Universities (Nos. N2216016 and N2316002), the Yunnan Fundamental Research Projects (No. 202401BC070021), and the Program of Introducing Talents of Discipline to Universities, Plan 111 (No.B16009).

References

Achiam, J.; Adler, S.; Agarwal, S.; Ahmad, L.; Akkaya, I.; Aleman, F. L.; Almeida, D.; Altenschmidt; et al. 2023. Gpt-4 technical report. *ArXiv preprint*.

AI, A. 2023. Fuyu-8b: A multimodal architecture for ai agents.

Aiello, E.; Yu, L.; Nie, Y.; Aghajanyan, A.; and Oguz, B. 2023. Jointly training large autoregressive multimodal models. *ArXiv preprint*.

Alayrac, J.-B.; Donahue, J.; Luc, P.; Miech, A.; Barr, I.; Hasson, Y.; Lenc, K.; Mensch, A.; Millican, K.; Reynolds, M.; et al. 2022. Flamingo: A visual language model for few-shot learning. *Proc. of NeurIPS*.

Awadalla, A.; Gao, I.; Gardner, J.; Hessel, J.; Hanafy, Y.; Zhu, W.; Marathe, K.; Bitton, Y.; Gadre, S.; Sagawa, S.; et al. 2023. Openflamingo: An open-source framework for training large autoregressive vision-language models. *ArXiv preprint*.

Bai, J.; Bai, S.; Yang, S.; Wang, S.; Tan, S.; Wang, P.; Lin, J.; Zhou, C.; and Zhou, J. 2023. Qwen-vl: A frontier large vision-language model with versatile abilities. *ArXiv preprint*.

Bai, Y.; Jones, A.; Ndousse, K.; Askell, A.; Chen, A.; Das-Sarma, N.; Drain, D.; Fort, S.; Ganguli, D.; Henighan, T.; et al. 2022. Training a helpful and harmless assistant with reinforcement learning from human feedback. *arXiv preprint arXiv:2204.05862*.

Bradley, R. A.; and Terry, M. E. 1952. Rank analysis of incomplete block designs: I. The method of paired comparisons. *Biometrika*.

Brown, T. B.; Mann, B.; Ryder, N.; Subbiah, M.; Kaplan, J.; Dhariwal, P.; Neelakantan, A.; Shyam, P.; Sastry, G.; Askell, A.; Agarwal, S.; Herbert-Voss, A.; Krueger, G.; Henighan, T.; Child, R.; Ramesh, A.; Ziegler, D. M.; Wu, J.; Winter, C.; Hesse, C.; Chen, M.; Sigler, E.; Litwin, M.; Gray, S.; Chess, B.; Clark, J.; Berner, C.; McCandlish, S.; Radford, A.; Sutskever, I.; and Amodei, D. 2020. Language Models are Few-Shot Learners. In *Proc. of NeurIPS*.

Burns, C.; Izmailov, P.; Kirchner, J. H.; Baker, B.; Gao, L.; Aschenbrenner, L.; Chen, Y.; Ecoffet, A.; Joglekar, M.; Leike, J.; et al. 2023. Weak-to-strong generalization: Eliciting strong capabilities with weak supervision. *ArXiv preprint*.

Chen, J.; Zhu, D.; Shen, X.; Li, X.; Liu, Z.; Zhang, P.; Krishnamoorthi, R.; Chandra, V.; Xiong, Y.; and Elhoseiny, M. 2023. Minigpt-v2: large language model as a unified interface for vision-language multi-task learning. *ArXiv preprint*.

Coste, T.; Anwar, U.; Kirk, R.; and Krueger, D. 2023. Reward model ensembles help mitigate overoptimization. *ArXiv preprint*.

Cui, G.; Yuan, L.; Ding, N.; Yao, G.; Zhu, W.; Ni, Y.; Xie, G.; Liu, Z.; and Sun, M. 2023. Ultrafeedback: Boosting language models with high-quality feedback. *ArXiv preprint*.

Devlin, J.; Chang, M.-W.; Lee, K.; and Toutanova, K. 2019. BERT: Pre-training of Deep Bidirectional Transformers for Language Understanding. In *Proc. of NAACL*.

Dubois, Y.; Li, C. X.; Taori, R.; Zhang, T.; Gulrajani, I.; Ba, J.; Guestrin, C.; Liang, P. S.; and Hashimoto, T. B. 2024. Alpacafarm: A simulation framework for methods that learn from human feedback. *Proc. of NeurIPS*, 36.

Eisenstein, J.; Nagpal, C.; Agarwal, A.; Beirami, A.; D’Amour, A.; Dvijotham, D.; Fisch, A.; Heller, K.; Pfohl, S.; Ramachandran, D.; et al. 2023. Helping or herding? reward model ensembles mitigate but do not eliminate reward hacking. *ArXiv preprint*.

Favero, A.; Zancato, L.; Trager, M.; Choudhary, S.; Perera, P.; Achille, A.; Swaminathan, A.; and Soatto, S. 2024. Multi-modal hallucination control by visual information grounding. In *Proc. of CVPR*.

Fernandes, P.; Farinhas, A.; Rei, R.; C. de Souza, J. G.; Ogayo, P.; Neubig, G.; and Martins, A. 2022. Quality-Aware Decoding for Neural Machine Translation. In *Proc. of NAACL*.

Gao, L.; Schulman, J.; and Hilton, J. 2023. Scaling laws for reward model overoptimization. In *Proc. of ICML*.

Gao, M.; Hu, X.; Ruan, J.; Pu, X.; and Wan, X. 2024. Llm-based nlg evaluation: Current status and challenges. *arXiv preprint arXiv:2402.01383*.

Gu, Y.; Tinn, R.; Cheng, H.; Lucas, M.; Usuyama, N.; Liu, X.; Naumann, T.; Gao, J.; and Poon, H. 2021. Domain-specific language model pretraining for biomedical natural language processing. *Proc. of HEALTH*.

Gunjal, A.; Yin, J.; and Bas, E. 2024. Detecting and preventing hallucinations in large vision language models. In *Proc. of AAAI*.

Gurumoorthy, K. S.; Jawanpuria, P.; and Mishra, B. 2021. SPOT: A framework for selection of prototypes using optimal transport. In *Proc. of KDD*.

Hong, J.; Lee, N.; and Thorne, J. 2024. Orpo: Monolithic preference optimization without reference model. *ArXiv preprint*.

Hu, E. J.; Shen, Y.; Wallis, P.; Allen-Zhu, Z.; Li, Y.; Wang, S.; Wang, L.; and Chen, W. 2022. LoRA: Low-Rank Adaptation of Large Language Models. In *Proc. of ICLR*.

Hu, J.; Yao, Y.; Wang, C.; Wang, S.; and Pan, e. 2023. Large multilingual models pivot zero-shot multimodal learning across languages. *ArXiv preprint*.

Huang, Q.; Dong, X.; Zhang, P.; Wang, B.; He, C.; Wang, J.; Lin, D.; Zhang, W.; and Yu, N. 2024a. Opera: Alleviating hallucination in multi-modal large language models via over-trust penalty and retrospection-allocation. In *Proc. of CVPR*.

Huang, S.; Dong, L.; Wang, W.; Hao, Y.; Singhal, S.; Ma, S.; Lv, T.; Cui, L.; Mohammed, O. K.; Patra, B.; et al. 2024b. Language is not all you need: Aligning perception with language models. *Proc. of NeurIPS*.

Kang, F.; Just, H. A.; Sun, Y.; Jahagirdar, H.; Zhang, Y.; Du, R.; Sahu, A. K.; and Jia, R. 2024. Get more for less: Principled Data Selection for Warming Up Fine-Tuning in LLMs. *ArXiv preprint*.

Lee, A.; Auli, M.; and Ranzato, M. 2021. Discriminative Reranking for Neural Machine Translation. In *Proc. of ACL*.

Leng, S.; Zhang, H.; Chen, G.; Li, X.; Lu, S.; Miao, C.; and Bing, L. 2024. Mitigating object hallucinations in large vision-language models through visual contrastive decoding. In *Proc. of CVPR*.

Li, L.; Xie, Z.; Li, M.; Chen, S.; Wang, P.; Chen, L.; Yang, Y.; Wang, B.; and Kong, L. 2023a. Silkie: Preference distillation for large visual language models. *ArXiv preprint*.

Li, Y.; Zhang, C.; Yu, G.; Wang, Z.; Fu, B.; Lin, G.; Shen, C.; Chen, L.; and Wei, Y. 2023b. Stablellava: Enhanced visual instruction tuning with synthesized image-dialogue data. *ArXiv preprint*.

Li, Y.; Zhang, Y.; Wang, C.; Zhong, Z.; Chen, Y.; Chu, R.; Liu, S.; and Jia, J. 2024. Mini-gemini: Mining the potential of multi-modality vision language models. *ArXiv preprint*.

Lin, J.; Yin, H.; Ping, W.; Molchanov, P.; Shoeybi, M.; and Han, S. 2024. Vila: On pre-training for visual language models. In *Proc. of CVPR*.

Liu, F.; Lin, K.; Li, L.; Wang, J.; Yacoob, Y.; and Wang, L. 2023. Aligning large multi-modal model with robust instruction tuning. *ArXiv preprint*.

Liu, H.; Li, C.; Li, Y.; and Lee, Y. J. 2024a. Improved baselines with visual instruction tuning. In *Proc. of CVPR*.

Liu, H.; Li, C.; Li, Y.; Li, B.; Zhang, Y.; Shen, S.; and Lee, Y. J. 2024b. LLaVA-NeXT: Improved reasoning, OCR, and world knowledge.

Liu, H.; Li, C.; Wu, Q.; and Lee, Y. J. 2024c. Visual instruction tuning. *Proc. of NeurIPS*.

Liu, J.; Huang, X.; Zheng, J.; Liu, B.; Wang, J.; Yoshie, O.; Liu, Y.; and Li, H. 2024d. MM-Instruct: Generated Visual Instructions for Large Multimodal Model Alignment. *ArXiv preprint*.

Liu, W.; Zhang, C.; Yu, B.; and Li, Y. 2019a. A general multi-source data fusion framework. In *Proc. of ICML*.

Liu, Y.; Ott, M.; Goyal, N.; Du, J.; Joshi, M.; Chen, D.; Levy, O.; Lewis, M.; Zettlemoyer, L.; and Stoyanov, V. 2019b. Roberta: A robustly optimized bert pretraining approach. *ArXiv preprint*.

Luce, R. D. 2005. *Individual choice behavior: A theoretical analysis*. Courier Corporation.

Meng, Y.; Xia, M.; and Chen, D. 2024. Simpo: Simple preference optimization with a reference-free reward. *ArXiv preprint*.

Ouyang, L.; Wu, J.; Jiang, X.; Almeida, D.; Wainwright, C.; Mishkin, P.; Zhang, C.; Agarwal, S.; Slama, K.; Ray, A.; et al. 2022. Training language models to follow instructions with human feedback. *Proc. of NeurIPS*.

Panigrahi, A.; Saunshi, N.; Zhao, H.; and Arora, S. 2023. Task-specific skill localization in fine-tuned language models. In *Proc. of ICML*.

Rafailov, R.; Sharma, A.; Mitchell, E.; Manning, C. D.; Ermon, S.; and Finn, C. 2024. Direct preference optimization: Your language model is secretly a reward model. *Proc. of NeurIPS*.

Rohrbach, A.; Hendricks, L. A.; Burns, K.; Darrell, T.; and Saenko, K. 2018. Object Hallucination in Image Captioning. In *Proc. of EMNLP*.

Schulman, J.; Wolski, F.; Dhariwal, P.; Radford, A.; and Klimov, O. 2017. Proximal policy optimization algorithms. *ArXiv preprint*.

Stiennon, N.; Ouyang, L.; Wu, J.; Ziegler, D. M.; Lowe, R.; Voss, C.; Radford, A.; Amodei, D.; and Christiano, P. F. 2020. Learning to summarize with human feedback. In *Proc. of NeurIPS*.

Sun, Z.; Shen, S.; Cao, S.; Liu, H.; Li, C.; Shen, Y.; Gan, C.; Gui, L.-Y.; Wang, Y.-X.; Yang, Y.; et al. 2023. Aligning large multimodal models with factually augmented rlhf. *ArXiv preprint*.

Touvron, H.; Martin, L.; Stone, K.; Albert, P.; Almahairi, A.; Babaei, Y.; Bashlykov, N.; Batra, S.; Bhargava, P.; Bhosale, S.; et al. 2023. Llama 2: Open foundation and fine-tuned chat models. *ArXiv preprint*.

Villani, C.; et al. 2009. *Optimal transport: old and new*. Springer.

Wang, C.; Zhou, H.; Chang, K.; Li, B.; Mu, Y.; Xiao, T.; Liu, T.; and Zhu, J. 2024a. Hybrid Alignment Training for Large Language Models. *ArXiv preprint*.

Wang, C.; Zhou, H.; Hu, Y.; Huo, Y.; Li, B.; Liu, T.; Xiao, T.; and Zhu, J. 2024b. Esrl: Efficient sampling-based reinforcement learning for sequence generation. In *Proc. of AAAI*.

Wang, F.; Zhou, W.; Huang, J. Y.; Xu, N.; Zhang, S.; Poon, H.; and Chen, M. 2024c. mDPO: Conditional Preference Optimization for Multimodal Large Language Models. *ArXiv preprint*.

Wang, J.; Wang, Y.; Xu, G.; Zhang, J.; Gu, Y.; Jia, H.; Yan, M.; Zhang, J.; and Sang, J. 2023. An llm-free multi-dimensional benchmark for mllms hallucination evaluation. *ArXiv preprint*.

Wang, W.; Chen, Z.; Chen, X.; Wu, J.; Zhu, X.; Zeng, G.; Luo, P.; Lu, T.; Zhou, J.; Qiao, Y.; et al. 2024d. Vision-llm: Large language model is also an open-ended decoder for vision-centric tasks. *Proc. of NeurIPS*.

Wang, Y.; Yao, Q.; Kwok, J. T.; and Ni, L. M. 2020. Generalizing from a few examples: A survey on few-shot learning. *ACM computing surveys (csur)*.

Wu, Z.; Hu, Y.; Shi, W.; Dziri, N.; Suhr, A.; Ammanabrolu, P.; Smith, N. A.; Ostendorf, M.; and Hajishirzi, H. 2024. Fine-grained human feedback gives better rewards for language model training. *Proc. of NeurIPS*.

Xia, M.; Malladi, S.; Gururangan, S.; Arora, S.; and Chen, D. 2024. Less: Selecting influential data for targeted instruction tuning. *ArXiv preprint*.

Xiao, T.; and Zhu, J. 2023. Introduction to Transformers: an NLP Perspective. *arXiv preprint arXiv:2311.17633*.

Xie, H.; Li, J.; and Xue, H. 2017. A survey of dimensionality reduction techniques based on random projection. *ArXiv preprint*.

Yu, T.; Yao, Y.; Zhang, H.; He, T.; Han, Y.; Cui, G.; Hu, J.; Liu, Z.; Zheng, H.-T.; Sun, M.; et al. 2024a. Rlhf-v: Towards trustworthy mllms via behavior alignment from fine-grained correctional human feedback. In *Proc. of CVPR*.

Yu, T.; Zhang, H.; Yao, Y.; Dang, Y.; Chen, D.; Lu, X.; Cui, G.; He, T.; Liu, Z.; Chua, T.-S.; et al. 2024b. Rlaif-v: Aligning mllms through open-source ai feedback for super gpt-4v trustworthiness. *ArXiv preprint*.

Zhao, Z.; Wang, B.; Ouyang, L.; Dong, X.; Wang, J.; and He, C. 2023. Beyond hallucinations: Enhancing lvlms through hallucination-aware direct preference optimization. *ArXiv preprint*.

Zhou, H.; Wang, C.; Hu, Y.; Xiao, T.; Zhang, C.; and Zhu, J. 2024a. Prior Constraints-based Reward Model Training for Aligning Large Language Models. *ArXiv preprint*.

Zhou, Y.; Cui, C.; Rafailov, R.; Finn, C.; and Yao, H. 2024b. Aligning modalities in vision large language models via preference fine-tuning. *ArXiv preprint*.

Zhou, Y.; Cui, C.; Yoon, J.; Zhang, L.; Deng, Z.; Finn, C.; Bansal, M.; and Yao, H. 2023. Analyzing and mitigating object hallucination in large vision-language models. *ArXiv preprint*.

Appendix A: Experimental Details

Settings

Best-of- n Sampling we employed top- p sampling with $p = 0.95$ and a temperature of 0.2 to generate eight candidate responses. We then picked the response with the highest reward score as the final output.

RL Training We trained the LVLM using PPO via the trlx implementation⁸. The learning rates were set at 1e-5 for the language model and 5e-6 for the value model. Each PPO step used a batch size of 32, with 15k gradient steps and two mini-batch update epochs. To address over-optimization, as noted by Gao, Schulman, and Hilton (2023), we saved checkpoints at regular intervals during training. Specifically, we evaluated checkpoints every 100 steps using our validation set and selected the one with the highest reward score. The validation set, randomly sampled from LLaVA-Instruct-150K, consisted of 1k samples. Following Zhou et al. (2024a) and Wang et al. (2024a), we also employed a cold-start trick for PPO, to alleviate the damage caused by the inaccurate estimation of the early value model. Specifically, we only updated the value model and did not update the policy model during the first 30 steps of RL training. Additionally, following Wang et al. (2024b)'s work, we standardized our reward scores using a reward queue, which stored the previous 1k reward scores to calculate the mean and variance. All of our experiments were done on eight A800 GPUs.

Preference Data Selection We utilized LoRA to pre-train the reward model, as described by Xia et al. (2024). For each preference sample, we then extracted 8192-dimensional gradient features from the pre-trained model.

DPO Training We used a batch size of 64, a learning rate of 1e-6, and trained for one epoch in DPO training. Except for these parameters, our setup matched Rafailov et al. (2024). In three-phase progressive training, the learning rate was 1e-6 in phase one and 5e-7 in phases two and three.

Random Projection We employed random projection to reduce the dimensionality of gradient features, illustrated here with the example of computing the gradient feature for a preference sample s_i . Initially, we concatenated all gradients from $\nabla \mathcal{L}_{reward}(s_i; \theta_{warmup})$ to form the gradient feature $g_i^{\text{init}} \in \mathbb{R}^{1 \times d}$, where d represents the number of trainable neurons. Although the LoRA training approach was employed to reduce d , it remained large. Therefore, random projection was applied to further reduce the dimensionality. Specifically, a random matrix R was first generated with dimensions $d \times k$, where k denotes the target dimensionality, significantly lower than d . The elements of R were typically drawn from a standard normal distribution $\mathcal{N}(0, 1)$. Then, the high-dimensional g_i^{init} was projected into a lower-dimensional space by computing the matrix product:

$$g_i = g_i^{\text{init}} \times R \quad (7)$$

According to the Johnson-Lindenstrauss Lemma (Xie, Li, and Xue 2017), random projection approximately preserved

the pairwise Euclidean distances between our gradient features with high probability.

Evaluation

In this section, we describe how we compute the WinRate for the MM-Instruct benchmark. Given the pairwise test responses $\{(x^0, r_a^0, r_b^0), \dots, (x^T, r_a^T, r_b^T)\}$, where T is the number of the test set, we employ GPT-4 to annotate the preference of each pairwise response, including P_a , P_b , and Tie . Here, P_a denotes response r_a is better than response r_b , P_b denotes response r_b is worse than response r_b , while Tie denotes a tie between response r_a and response r_b . To address potential location bias in the evaluation (Gao et al. 2024), we conduct two separate evaluations for each pair, alternating the order of r_a and r_b . The final result is based on the evaluations where the preferences align consistently. We can compute the WinRate for the models generating responses r_a and r_b based on these annotated preferences:

$$S_{\text{WinRate}}^a = \frac{\text{Count}(P_a)}{T - \text{Count}(Tie)} \quad (8)$$

$$S_{\text{WinRate}}^b = \frac{\text{Count}(P_b)}{T - \text{Count}(Tie)} \quad (9)$$

where $\text{Count}(\cdot)$ represents the number of occurrences of the specified preference.

Image Caption Annotation

For image caption annotation, we employed a template similar to that proposed by Liu et al. (2024c). However, this approach raises two concerns: the potential unreliability of the annotations and associated ethical risks. First, GPT-4o is widely regarded as a highly effective visual model, with its smaller variant, GPT-4o-mini, demonstrating comparable performance on image caption tasks across multiple publicly available benchmarks, such as Object HalBench and AMBER (see Table 1). Furthermore, GPT-4o-mini is significantly more cost-effective. Given these factors, we consider GPT-4o-mini to be reliable and select it for our annotation process. Second, ethical and moral risks are not a concern since the images are derived from open datasets, and GPT-4o functions as an open multimodal LLM.

We employed Vision-LLM-Alignment⁹ to train our RoVRM, and performed best-of- n sampling, RL training, and DPO training.

Appendix B: More Analysis

Comparison with Other Preference Data Selection Approaches To validate the effectiveness of using optimal transport in our preference data approach, we compare it with other distance computation approaches. Specifically, we examine alternative ways of calculating the distance score in Eq. 5, such as **Cosine Similarity**, Kullback-Leibler divergence (**KL**), and **L_2 -norm**, instead of the optimal transport function $OT(\cdot)$. The results are summarized in Table 5. From the results, we can observe that optimal transport significantly outperforms other approaches in preference

⁸<https://github.com/CarperAI/trlx>

⁹<https://github.com/wangclnlp/Vision-LLM-Alignment>

Method	Best-of- n Sampling		Reinforcement Learning	
	AMBER (HalRate \downarrow)	LLaVA ^W (Score \uparrow)	AMBER (HalRate \downarrow)	LLaVA ^W (Score \uparrow)
VRM-Vanilla	29.0	73.6	29.1	72.8
RoVRM				
+ Cosine Similarity	25.7	78.9	25.2	75.1
+ KL	26.4	75.4	28.5	72.2
+ L_2 -norm	27.9	76.6	26.0	74.3
+ Optimal Transport	23.9	82.0	23.4	78.3

Table 5: Performance on the best-of- n sampling and RL training with reward models trained via various preference data selection approaches.

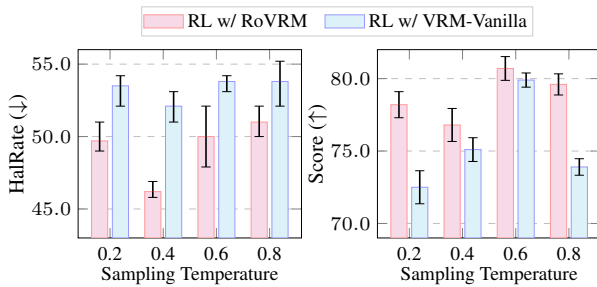


Figure 6: Performance of the RL-trained LLaVA-1.5-7B model at temperature settings of 0.2, 0.4, 0.6, and 0.8.

data selection. This superiority underscores its effectiveness in identifying relevant textual preferences for training RoVRM, as optimal transport more accurately captures the transfer distance of preferences, whereas other approaches primarily measure similarity.

Performance on Different Temperature Settings Different temperature settings typically yield varying responses when applying an LViM. To evaluate this comprehensively, we also compare the RoVRM and VRM-Vanilla under different temperature settings, as shown in Figure 6. The results indicate that RoVRM surpasses RL’s best-case performance on the MMHalBench and LLaVA-Bench benchmarks. This highlights the benefit of integrating textual preference data into VRM training.

Performance on Different Textual Preference Datasets The performance of our RoVRM depends on the quality of the textual preference dataset. Therefore, in addition to UltraFeedback, we also evaluate RoVRM on other general textual preference datasets, including the Alpaca preference dataset (Dubois et al. 2024) and Helpful preference dataset (Bai et al. 2022). Additionally, we evaluate RoVRM on a fusion of these datasets. The preference data selection process, as described in Section **Preference Data Selection**, is applied to all datasets. Our results show that, compared to VRM-Vanilla, utilizing each of these textual preference datasets improves the VRM’s robustness, further validating the effectiveness of our three-phase progressive training and preference data selection methods. Moreover, the results show that UltraFeedback yields the most significant performance gains, outperforming Alpaca and Helpful, likely due to its larger data scale. Interestingly, although the Helpful

Method	Num.	AMBER		LLaVA ^W	MMIns
		Cover. \uparrow	HalRate \downarrow	Score \uparrow	WinRate \uparrow
LLaVA-1.5-7B	-	50.3	37.1	66.7	46.16
Best-of-n Sampling					
VRM-Vanilla	-	50.8	29.0	73.6	57.69
RoVRM					
+Alpaca	10k	50.7	26.0	80.6	58.72
+Helpful	44k	50.8	26.6	79.3	57.44
+UltraFeedback	340k	53.2	23.9	82.0	61.91
+Fusion	394k	51.1	26.4	82.5	60.71
Reinforcement Learning					
VRM-Vanilla	-	49.1	29.1	72.8	51.11
RoVRM					
+Alpaca	10k	46.8	26.5	76.7	56.92
+Helpful	44k	49.5	32.7	75.8	46.95
+UltraFeedback	340k	48.2	23.4	78.3	58.69
+Fusion	394k	44.1	21.0	77.9	59.00

Table 6: Performance on different textual preference datasets is evaluated using the LLaVA-1.5-7B model. “Num.” refers to the number of comparison preference pairs in each textual preference dataset.

Method	Best-of- n Sampling		Reinforcement Learning	
	AMBER (HalRate \downarrow)	LLaVA ^W (Score \uparrow)	AMBER (HalRate \downarrow)	LLaVA ^W (Score \uparrow)
P1&P2→P3	26.5	76.9	28.1	70.9
P1→P2&P3	26.6	76.7	25.8	72.2
P1&P2&P3	31.1	74.1	38.5	68.0
P1→P2→P3	23.9	82.0	23.4	78.3

Table 7: Performance on the LLaVA-1.5-7B model with different preference data fusion strategies. & denotes the combination of two preference datasets. → denotes a two-step training process: first, the VRM is trained with the former preference dataset at a higher learning rate, followed by the latter preference dataset at a lower learning rate. P1, P2, and P3 denote the three phases depicted in Figure 1, respectively.

dataset is also sizable, it does not outperform Alpaca. This discrepancy may be due to the Helpful dataset’s emphasis on helpfulness, which could limit its ability to capture a broader spectrum of human preferences. Furthermore, the results from the fusion show a slight improvement over certain benchmarks, such as LLaVA-Bench on the best-of- n sampling. However, we chose not to use the fusion in this work, as the performance gains were minimal and inconsistent across all benchmarks. Additionally, the fusion data incurs higher computational costs, increasing the workload of our research.

Comparison with Preference Data Fusion Data fusion from multiple sources is a common approach to achieving knowledge transfer (Liu et al. 2019a). Intuitively, one approach to transferring preferences from text is to combine textual and visual preference datasets. Thus, we also compare various data fusion strategies with three-phase progressive training in Table 7. The results indicate that data fusion strategies are less effective than the three-phase progressive training, likely due to the inherent challenges of optimizing

Method	#Param	MMHalBench		Object HalBench		AMBER		LLaVA ^W	MMIns
		Score \uparrow	HalRate \downarrow	Resp. \downarrow	Ment. \downarrow	Cover. \uparrow	HalRate \downarrow	Score \uparrow	WinRate \uparrow
Best-of-n Sampling									
LLaVA-NeXT-7B	7B	2.59	50.0	16.0	10.6	61.8	52.8	85.7	90.70
+VRM-Vanilla	7B	2.61	48.0	14.7	9.1	60.9	44.3	99.1	95.40
+RoVRM-Random	7B	2.68	46.3	12.5	8.2	60.4	38.6	102.8	97.67
+RoVRM	7B	2.77	45.8	10.3	6.2	59.2	32.8	106.1	100.00
LLaVA-NeXT-13B	13B	2.71	49.0	14.0	9.0	62.0	54.4	100.5	92.13
+VRM-Vanilla	13B	2.79	47.9	12.7	8.3	59.3	44.0	100.8	93.33
+RoVRM-Random	13B	2.70	46.5	12.1	7.8	59.7	42.5	101.3	95.56
+RoVRM	13B	2.85	44.8	10.7	6.5	61.2	40.2	102.4	100.00
Reinforcement Learning									
LLaVA-NeXT-7B	7B	2.59	50.0	16.0	10.6	61.8	52.8	85.7	90.70
+VRM-Vanilla	7B	2.68	45.8	13.7	8.9	50.9	34.2	87.1	93.67
+RoVRM-Random	7B	2.70	41.5	11.7	8.3	53.8	39.4	89.0	94.94
+RoVRM	7B	2.81	38.0	10.8	7.6	55.0	30.3	91.7	96.20
LLaVA-NeXT-13B	13B	2.71	49.0	14.0	9.0	62.0	54.4	100.5	92.13
+VRM-Vanilla	13B	2.85	45.2	11.8	8.9	56.8	34.7	101.5	94.79
+RoVRM-Random	13B	2.96	41.3	12.1	8.6	55.6	31.1	103.0	95.56
+RoVRM	13B	3.14	37.8	10.1	5.8	57.2	30.9	106.7	96.88

Table 8: Experimental results on the LLaVA-NeXT-7B and -13B models.

Phase	Sample	Device	Time Cost
Phase One			
Warmup Training	5k	1 \times GPU	2.40h
Gradient Feature	58k	8 \times GPU	2.55h
Optimal Transport	57k	1 \times CPU	0.55h \sim 0.75h
Phase Two			
Warmup Training	5k	1 \times GPU	2.02h
Gradient Feature	100k	8 \times GPU	3.26h
Optimal Transport	95k	1 \times CPU	0.55h \sim 0.75h

Table 9: Time costs associated with preference data selection are reported. The “Sample” column indicates the number of processed preference samples at each step. Due to variations in CPU processing speed, influenced by the number of active tasks or cores, we present a range of time costs derived from multiple experiments.

the ratio between the datasets. This advantage in progressive training aligns with recent advancements in applying LLMs to specific tasks, where models are initially fine-tuned with general instruction data, followed by task-specific instruction data, rather than using a fusion approach (Panigrahi et al. 2023; Gu et al. 2021).

Performance on Different LVLMs To further validate the generalizability of our RoVRM, we conduct additional experiments using the LLaVA-NeXT (as known as LLaVA-1.6) models which improve input image resolution and use an improved visual instruction tuning data (Liu et al. 2024b). The experimental results, presented in Table 8, consistently demonstrate that RoVRM outperforms VRM-Vanilla in both best-of- n sampling and RL training, mirroring the findings in Table 1. Notably, during RL training with RoVRM, LLaVA-NeXT-13B achieves 106.7 points on the LLaVA-

Bench. Although LLaVA-NeXT models are already robust compared to LLaVA-1.5, RoVRM continues to improve their performance, indicating that the preferences learned by RoVRM are distinct from those captured by strong supervised fine-tuning. This demonstrates the effectiveness of our proposed approaches to learning preferences.

Time Costs for Preference Data Selection Table 9 provides the time required for our preference data selection. The test is performed on eight A800 GPUs and an Intel Xeon Platinum 8358P CPU. The results demonstrate that our approach incurs minimal time costs, ensuring its feasibility for real-world applications.

Case Study We provide several qualitative examples in Figures 7 and 8 to illustrate the impact of RoVRM on aligning the LLaVA-1.5-7B model with human preferences. These examples highlight RoVRM’s ability to generate more truthful and helpful responses.

<p>Instruction: <image>\n What is the brand of the yogurt flavored with blueberry?</p> <p>Best-of-<i>n</i> Sampling w/ VRM-Vanilla: The brand of the yogurt flavored with blueberry is “Chobani”.</p> <p>Best-of-<i>n</i> Sampling w/ RoVRM: The yogurt is flavored with blueberries, but I cannot determine the brand without more specific information.</p>	
<p>Instruction: <image>\n This is the logo of LLaVA, Large Language and Vision Assistant, based on the LLaMA architecture. Please explain this logo in detail, and how do you think of its design.</p> <p>RL Training w/ VRM-Vanilla: The LLaVA logo is a unique and creative design that features a fire-breathing, flaming red horse or pony. The horse's eyes are wearing glasses, adding a whimsical touch to the image. The combination of the fire and the glasses gives the impression of a futuristic and imaginative creature. The design of the LLaVA logo is both visually striking and memorable, making it an effective representation of the brand.</p> <p>RL Training w/ RoVRM: The logo for LLaVA, Large Language and Vision Assistant, features an orange and red fire-breathing llama with glasses. The llama's design is creative and visually appealing, making it an interesting and memorable logo. The combination of the llama's fiery appearance and the glasses adds a unique touch to the logo, suggesting that the company behind it might be innovative and unconventional in its approach. The logo likely represents the company's focus on language and vision technology, with the llama symbolizing the fusion of these two aspects. Overall, the design of the logo is engaging and thought-provoking, reflecting the company's values and mission.</p>	

Figure 7: Examples where RoVRM can yield greater trustworthiness compared to VRM-Vanilla.

<p>Instruction: <image>\n Craft a concise caption capturing subjects' fashion essence in the given image.</p> <p>Best-of-<i>n</i> Sampling w/ VRM-Vanilla: A man in a white suit and a red tie walks down a runway at a fashion show, while other people are present around him, some of them holding handbags. The man's outfit, including the jacket and tie, adds a touch of sophistication and elegance to the scene.</p> <p>Best-of-<i>n</i> Sampling w/ RoVRM: The image showcases a man wearing a white suit, white jacket, and tie, standing on a runway with a blurry audience in the background. The man appears to be walking confidently, likely showcasing his fashion sense and style. He is holding a briefcase and wearing a lapel flower, which adds a touch of elegance to his ensemble. The scene conveys a sense of sophistication and confidence, as the man stands out and showcases his fashion choices to the audience.</p>	
<p>Instruction: <image>\n What's the ending of this movie?</p> <p>RL Training w/ VRM-Vanilla: The ending of this movie is not provided, as it is a scene from a movie or a romantic moment between two people on a boat.</p> <p>RL Training w/ RoVRM: The ending of this movie, "Titanic," is a tragic one, as the main characters, Jack and Rose, are unable to escape the sinking ship in time. Despite their love for each other, they are separated by the disaster, and Rose ultimately survives the ordeal. The film ends with Rose, now an elderly woman, looking at a painting of Jack, reflecting on their past and the love they shared.</p>	

Figure 8: Examples where RoVRM can yield greater helpfulness compared to VRM-Vanilla.